Geophysical Journal International

*Geophys. J. Int.* (2011) **187,** 1076–1088 doi: 10.1111/j.1365-246X.2011.05198.x

# The São Vicente earthquake of 2008 April and seismicity in the continental shelf off SE Brazil: further evidence for flexural stresses

M. Assumpção,[1] J. C. Dourado,[2] L. C. Ribotta,[3] W. U. Mohriak,[4,*] Fábio L. Dias[1] and J. R. Barbosa[1]

[1]*IAG, University of São Paulo, Rua do Matão* 1226, *São Paulo, SP,* 05508–090, *Brazil. E-mail: marcelo@iag.usp.br*
[2]*IGCE- UNESP, State University of São Paulo, Av.* 24-A 1515, *Rio Claro, SP,* 13506-900, *Brazil*
[3]*IPT, Technological Research Institute, São Paulo, SP,* 05508-901, *Brazil*
[4]*Petrobras, Rio de Janeiro, RJ, Brazil*

Accepted 2011 August 21. Received 2011 August 14; in original form 2011 March 30

## SUMMARY

The continental margin and shelf of most stable intraplate regions tend to be relatively more seismically active than the continental interior. In the southeast continental margin of Brazil, a seismic zone extends from Rio Grande do Sul to Espírito Santo, with seismic activity occurring mainly along the continental slope and suggesting a close relationship with flexural stresses caused by the weight of the sediments. In this region, earthquakes with magnitudes larger than 5 $m_b$ occur every 20–25 yr, on average. The focal mechanism solutions of previous earthquakes in this zone indicated reverse faulting on planes dipping approximately 45° with horizontal *P*-axes. The recent 5.2 $m_b$ earthquake of 2008 April 23 occurred 125 km south of São Vicente and was well recorded by many stations in SE Brazil, as well as at teleseismic distances in North America and Africa. Its focal depth was 17 km, locating the hypocentre in the lower crust. A well-determined focal mechanism solution shows one vertical nodal plane and one subhorizontal nodal plane. The *P*- and *T*-axes exhibit large dips, which were confirmed by a regional moment tensor inversion. This unusual orientation of the fault mechanism can be attributed to a rotation of the principal stress directions in the lower crust caused by flexural effects due to the load of recent sedimentation.

**Key words:** Earthquake source observations; Seismicity and tectonics; Intra-plate processes; Lithospheric flexure; South America.

## 1 INTRODUCTION

Passive margin earthquakes are an important type of intraplate seismicity, not only because continental shelf and coastal earthquakes account for one-third to one-quarter of all seismicity in stable continental crust (Johnston 1989; Schulte & Mooney 2005), but also because of the increasing seismic risk in many oil-rich continental shelves. Increased population in coastal areas also makes continental shelf seismicity an important issue in seismic hazard evaluation.

Since Sykes (1978) suggested a relationship between intraplate earthquakes and crustal 'zones of weakness', much progress has been made in understanding the seismicity of stable plate interiors. Johnston (1989) and Johnston & Kanter (1990) showed that 70 per cent of all large intraplate earthquakes (magnitudes > 6 $M_s$) occurred in extended (and presumably weak) crust such as passive margins and Mesozoic rifts. A more recent catalogue of intraplate earthquakes (Schulte & Mooney 2005) confirmed these findings and showed that 50 per cent of all events larger than magnitude 4.5 are associated with extended crust (interior rift and rifted continental margins). Rupture in pre-existing, and therefore weak, faults likely explain most intraplate earthquakes, as demonstrated by Zoback (1992) for North America by analysing the focal mechanisms in relation to the crustal stresses. Stein *et al.* (1989) emphasized that most mechanisms that have been proposed to explain passive margin seismicity (stresses from continent/ocean density contrasts; flexure due to sediment loading; ridge-push stresses) should produce seismicity in all passive margins, but this does not appear to be the case. Some passive margins are more active than others, especially those undergoing rebound from the unloading of the last ice age, such as the Canadian Atlantic coast. In the Norwegian continental margin, besides flexural stresses from glacial rebound, stresses from erosion/sedimentation also seem to contribute significantly to the seismicity (Bungum *et al.* 2010).

Fig. 1(a) shows the seismicity in SE Brazil. To evaluate better the geographical distribution of this seismicity, we filtered the Brazilian Earthquake Catalogue according to magnitude thresholds that vary with time. We used similar thresholds of Assumpção (1998a), that is, included all events with magnitude larger than 5.5 since approximately 1920 (which would be felt in large areas of the coast), larger than 5.0 since 1962 (well covered by the worldwide seismographic network), larger than 4.5 since 1970 (due to the installation of the

*Now at: Rio de Janeiro State University, Geology Dept., Rio de Janeiro, RJ, 20550-900, Brazil.



© 2011 The Authors
Geophysical Journal International © 2011 RAS

GJI Geodynamics and tectonics

Downloaded from http://gji.oxfordjournals.org/ at Universidade Estadual Paulista JÃºlio de Mesquita Filho on July 30, 2013

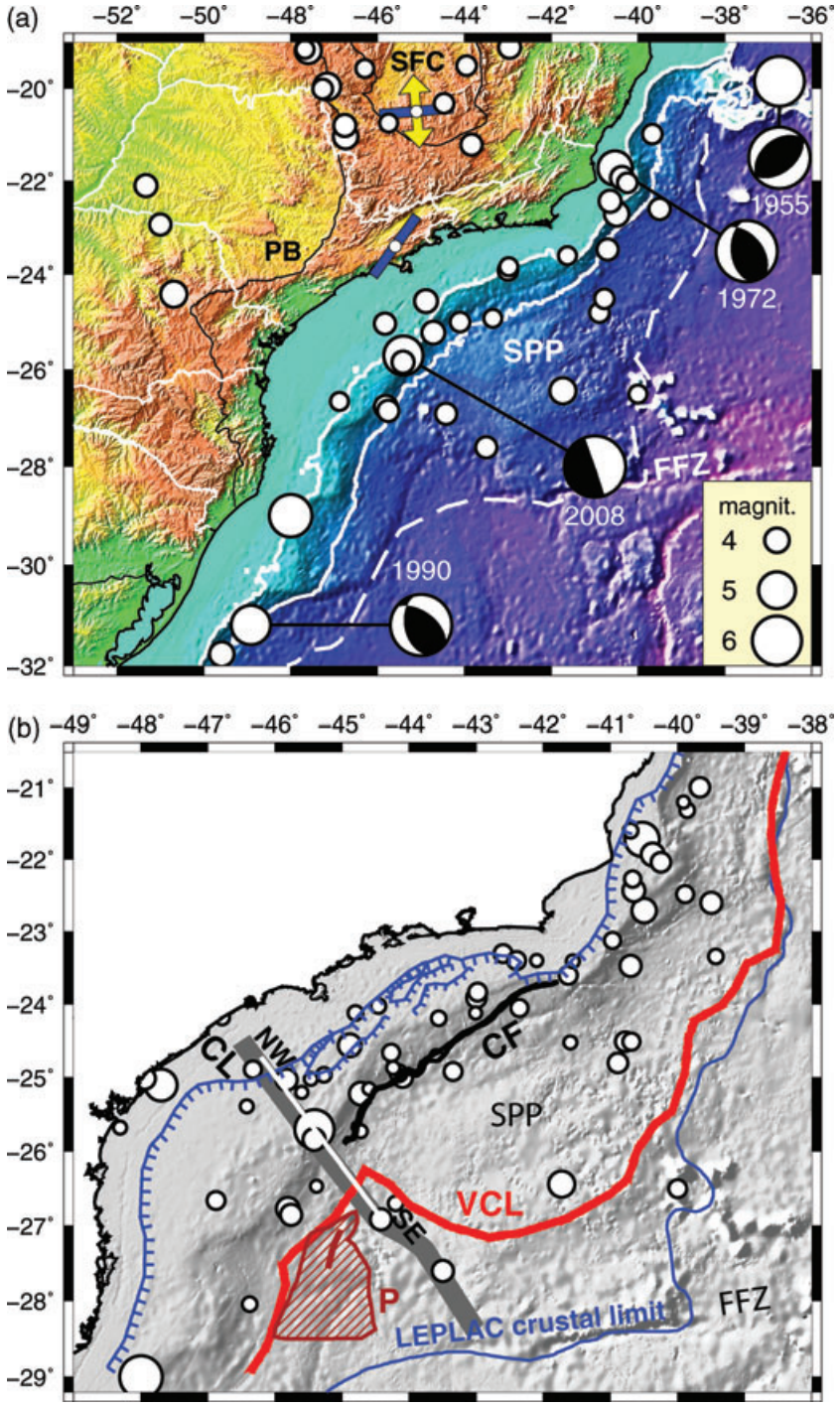



**Figure 1.** (a) Seismicity in SE Brazil. Solid white lines in the ocean are depth contours of 200 and 2000 m roughly defining the continental slope. The dashed white line indicates the limit of the continental extended crust, according to Leplac project (Gomes 1992). Open circles are epicentres of the uniform catalogue (see text). Note seismic activity trend along the continental slope (approximately between the 200 and 2000 m isodepths), where total sediment thickness tends to be larger. Focal mechanisms are from Mendiguren & Richter (1978) and Assumpção (1998a). Solid black lines in the continent are limits of the Paraná basin (PB) and the São Francisco craton (SFC). SPP is the São Paulo plateau, FFZ is the Florianópolis fracture zone. Blue bars and yellow arrows indicate Shmax and Shmin stresses, respectively (Assumpção 1998b). (b) Main structural features of the Santos basin. Dented blue lines denote the basin border faults at the hinge zone; CF is the Cabo Frio fault; SPP is the São Paulo plateau; the red line (VCL) is the volcanic crustal limit (Mohriak *et al.* 2010) defined by the presence of SDRs; the solid blue line is the proposed continental/oceanic crustal limit based on LEPLAC seismics and gravity data (Gomes 1992). The hachured brown area (*P*) is the rift propagator around the Abimael ridge, the probable termination of the northward propagating Atlantic opening, before the ridge jump to the east roughly along the Florianópolis fracture zone (FFZ), interpreted as a wedge of oceanic crust (Mohriak *et al.* 2010). Open circles are epicentres of the 'whole' catalogue (including old events with uneven geographical coverage). Thick grey line CL is the Capricornio Lineament. The white line NW–SE shows the location of the geoseismic transect of Fig. 7.

Downloaded from http://gji.oxfordjournals.org/ at Universidade Estadual Paulista JÃºlio de Mesquita Filho on July 30, 2013

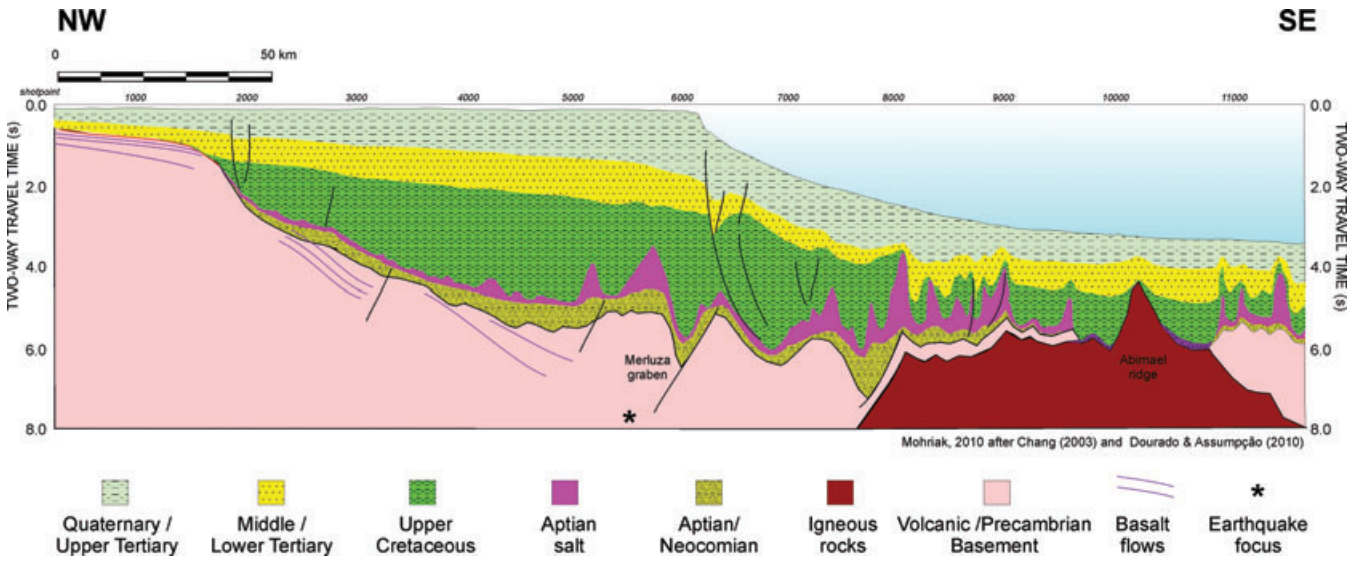



**Figure 2.** Schematic geoseismic transect from the continental platform of central Santos Basin towards the deep-water region, showing simplified stratigraphy of the rift, transitional and drift sequences. The location of the 2008 earthquake hypocentre in the lower crust is shown by a star near the shelf break, close to the Merluza graben. Interpretation based on Mohriak *et al.* 2010 (after Chang 2003; Dourado & Assumpção 2010, 2011).

Brasilia array station) and larger than 3.5 since 1980 (covered by the regional stations in SE Brazil). Such time-variable thresholds avoid oversampling more populated areas in the continent (locations with more records of old earthquakes felt by the population) as well as the continental shelf closer to São Paulo and Rio de Janeiro states, where seismographic stations have been operating since the early 1970s. This filtered catalogue (the 'uniform catalogue'), seen in Fig. 1(a), better shows which areas are more or less seismically active. Epicentral accuracy varies from approximately ±100 km, for small events located only by the regional stations in the continent (Assumpção 1998a) to approximately ±20 km for magnitude ∼5 earthquakes that have been identified by international agencies.

Fig. 1(a) shows a clear concentration of epicentres roughly along the continental slope (i.e. the seafloor area with the steepest slope, roughly between 200 and 2000 m bathymetry) where the largest sediment thicknesses are expected. The seismicity in the continent is separated from that of the continental margin, indicating different seismic zones with different sources of stress. A strike-slip stress regime (i.e. the intermediate principal stress is vertical) with E–W compression and N–S extension characterize the seismic zone in the southern part of the São Francisco craton and the surrounding Brasilia foldbelt (Assumpção 1998b). Earthquakes in the continental shelf and slope are predominantly due to reverse faulting, but the orientation of the compressional direction (Shmax) is not well known because the azimuths of the nodal planes are not well constrained (Assumpção 1998a). Note also that the extended and submerged continental crust, as defined by the dashed line in Fig. 1(a) (Chang *et al.* 1992; Gomes 1992), contains the small events in the oceanic part. Interestingly, the Serra do Mar coastal ranges are presently quite aseismic, despite clear evidence of neotectonism in the Pleistocene (Riccomini & Assumpção 1999).

The main structural features of the Santos basin are shown in Fig. 1(b), together with all known offshore epicentres of the 'whole', unfiltered catalogue. Most of the epicentres are located near the pre-Aptian limit of the continental margin basins marked by the proximal rift border faults and along the Cabo Frio Fault Zone in the Santos Basin (dented blue line and solid black line, respectively, in Fig. 1b). The Florianópolis Fracture Zone (FFZ) is marked by an E–W lineament. It has been associated with volcanic basement (Mohriak 2001, 2004) or with exhumed mantle (Gomes *et al.* 2008; Zalán *et al.* 2009). The limit of the submerged, extended continental crust is still under debate. Chang *et al.* (1992) and Gomes (1992) analysed seismic and gravity data and traced the limit of the continental/oceanic transition as shown by the Leplac line in Fig. 1(b). Mohriak *et al.* (2010) mapped the occurrence of SDRs (seaward-dipping reflectors) and proposed a different 'volcanic crustal limit' (VCL in Fig. 1b). The Abimael Ridge (in the brown hatched area of Fig. 1b) has been interpreted as an oceanic propagator, which advanced from the Pelotas Basin in the south towards the southern Santos Basin (Mohriak 2001; Carminatti *et al.* 2008; Mohriak *et al.* 2008), but failed to advance further northwards and was aborted in the Late Aptian. This caused a ridge jump roughly along the Florianopolis fracture zone and around the São Paulo plateau (Bueno 2004; Mohriak *et al.* 2010). Thus, the area between the volcanic limit and the Leplac line is probably continental crust, and the previous observation that offshore seismicity occurs predominantly in the extended, submerged continental crust is confirmed.

A regional geoseismic transect extending from the pre-Aptian limit of the basin towards the deep-water region is shown in Fig. 2 (transect location shown in Fig. 1b) based on data from Mohriak *et al.* 2010 (after Chang 2003; Dourado & Assumpção 2010, 2011). It illustrates the rift architecture and the salt tectonics styles in the margin, which are characterized by basinward sliding of post-salt blocks and by large diapirs affected by compression in the deep-water region (Cobbold *et al.* 1995; Mohriak *et al.* 1995). The oceanic propagator (Abimael ridge) separated two salt provinces, the larger one corresponding to the main salt province in the Santos Basin, and the smaller one ruptured by igneous intrusions and possibly by incipient seafloor spreading.

Magnitude statistics in the SE continental shelf (Fig. 3) indicate that earthquakes with magnitude 5 or larger occur every 20–25 yr, on average. The previous large events shown in Fig. 1 occurred in 1939 (Sta. Catarina, 5.5 $m_b$), 1955 (Espirito Santo, 6.1 $m_b$), 1972 (Rio de Janeiro, 4.8 $m_b$) and 1990 (Rio Grande do Sul, 5.2 $m_b$ ). The 2008 São Vicente earthquake with 5.2 $m_b$ was not an unexpected event.

Assumpção (1998a) showed that the seismicity in the SE continental shelf could be explained by the superposition of a regional



Downloaded from http://gji.oxfordjournals.org/ at Universidade Estadual Paulista JÃºlio de Mesquita Filho on July 30, 2013

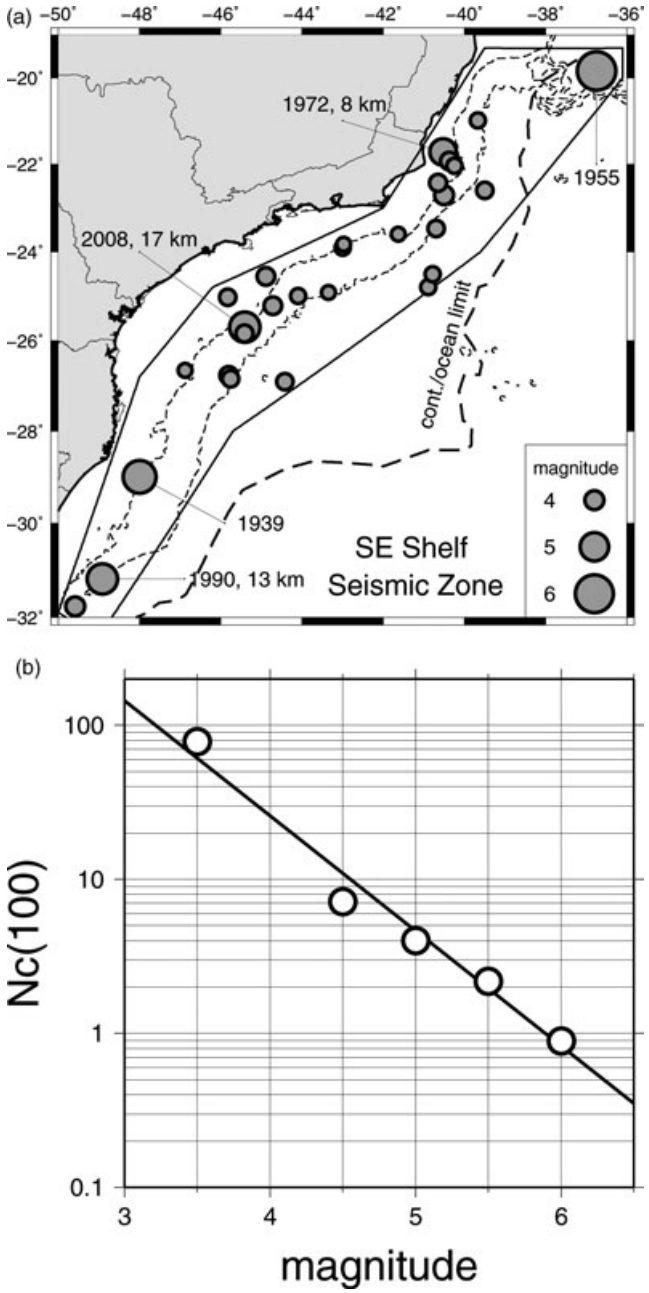



**Figure 3.** Magnitude statistics for the seismic zone of the SE continental shelf. (a) Polygon defining the limits of the seismic zone. Fine dashed line is the continental slope; long-dashed line is the continental/oceanic crustal transition. (b) Cumulative number of events (Nc) normalized for a period of 100 yr, according to the time-variable magnitude thresholds defined in the 'Introduction' section. Earthquakes larger than 5 $m_b$ occur once every 20–25 yr, on average.

plate-wide stress, caused by ridge-push and plate collisional forces, with local sources of stress, which are caused by (1) gravitational spreading stresses from continental/oceanic crustal transition and (2) flexure from sediment load. In addition, the extended crust from the Atlantic Mesozoic rifting processes could be weaker and more prone to failure under the present stresses. Here we study the hypocentral depth and the faulting mechanism of the recent 2008 São Vicente earthquake to contribute to a better characterization of the seismicity pattern in the SE continental shelf and the importance of flexural stresses.

## 2 LOCATION AND MAGNITUDE OF THE SÃO VICENTE EARTHQUAKE

### 2.1 Epicentre

Table 1 and Fig. 4 show the epicentre of the earthquake according to different international agencies (ISC 2011). The epicentral determinations of the U.S. Geological Survey (USGS) and the International Seismological Centre (ISC) have uncertainties of approximately ±5 km. These values, however, underestimate true uncertainty because they only indicate the scatter of the reading errors and assume a 1-D model of the Earth. Systematic errors due to lateral variations in the Earth's velocity structure can make the epicentral error somewhat larger, by approximately 20 km or more. The USGS and ISC epicentres were determined with a fixed depth of 10 km. Using the correct depth (17 km, as shown below) would not affect the epicentral location but only add ∼1.0 s in the earthquake origin time. Given the large number of stations and good azimuthal coverage of the reporting stations, the true accuracy of the ISC epicentre is expected to be less than 25 km at the 90 per cent confidence level, as indicated by the analysis of all ISC routine determinations carried out by Bondár *et al.* (2003).

The earthquake was well recorded by several stations in SE Brazil. We calculated an epicentre using the closest stations (Fig. 4) with very clear *P* wave first motions (upper-mantle refracted Pn phase). Some of these stations also recorded clear *S*-wave arrivals in the transverse component (SH waves). Fig. 5(a) shows that the SH onset is consistently negative (i.e. the polarity of the first motion is to the left, as indicated by the arrows in Fig. 4a). Using these *Sn* and *Pn* arrivals, a regional *Vp*/*Vs* ratio of 1.71 ± 0.04 was estimated (Fig. 5b). We tried two velocity models: (1) the BR model (Kwitko & Assumpção 1990) generally used to locate earthquakes in Brazil, with a *Vp*/*Vs* ratio of 1.74, and (2) a modification of the BR model with *Vp*/*Vs* of 1.71, and a crustal thickness of 31 km (the average between the ∼42 km crustal thickness beneath the stations and the ∼20 km crust at the epicentre). In addition, the Pn (upper-mantle *P* wave) velocity was reduced from 8.2 (BR model) to 8.0 because of known low-velocity anomalies in this area of SE Brazil (Feng *et al.* 2007; Rocha *et al.* 2011). These two epicentral solutions (BR74 and A71) were calculated with the HYPO71 code and are shown in Fig. 4(b) and Table 1. Again, the epicentral error bounds only reflect the traveltime residuals in relation to the 1-D model and do not take into account effects from 3-D structural variations. The epicentre obtained from these regional stations is little affected by the *P*-wave velocities of the 1-D model (whether BR or A) and are more affected by the *Vp*/*Vs* ratio. A change of ±0.04 in the *Vp*/*Vs* ratio moves the epicentre ±10 km north or south, respectively. The Wadati diagram (Fig. 5b) gives some indication of lateral variations in the *Vp*/*Vs* ratio. If corrections for this difference were taken into account, the local epicentre A71 would move eastwards, further away from the ISC epicentre.

Given the uncertainties in the velocity model, it is clear that the epicentre cannot be determined with an accuracy better than ±20–25 km. However, it is clear that the earthquake occurred very close to the continental slope, similar to the other events with magnitude ∼5 seen in Fig. 1. Its approximate location (25° 40′ S, 45° 25′ W) indicates that the epicentre lies within the bathymetric range of 200–600 m.

### 2.2 Magnitude

Two teleseismic magnitudes are commonly determined by international agencies: $m_b$ using teleseismic *P* waves with periods at



Downloaded from http://gji.oxfordjournals.org/ at Universidade Estadual Paulista JÃºlio de Mesquita Filho on July 30, 2013

**Table 1.** Epicentral determinations of the São Vicente Earthquake of 2008 April 23. Sources: ISC (International Seismological Centre, UK); NEIC (National Earthquake Information Center, US Geol. Survey). See text for BR74 and A71. Depth is fixed for every solution. RMS is the rms traveltime residual. *N* is the number of arrivals used in the determinations.

| Source | Latitude (°) | Longitude (°) | Error (km) | Depth (km) | RMS (s) | *N* | Origin Time (UT) (hh:min:sec) |
|---|---|---|---|---|---|---|---|
| ISC | 25.6496 | 45.4744 | 4.8 | 10 | 0.78 | 595 | 00:00:48.6 |
| NEIC | 25.7600 | 45.4690 | 6.2 | 10 | 0.91 | 218 | 00:00:47.8 |
| BR74 | 25.5983 | 45.3205 | 5.5 | 17 | 0.78 | 13 | 00:00:48.0 |
| A71 | 25.7045 | 45.2738 | 4.5 | 17 | 0.47 | 13 | 00:00:47.7 |

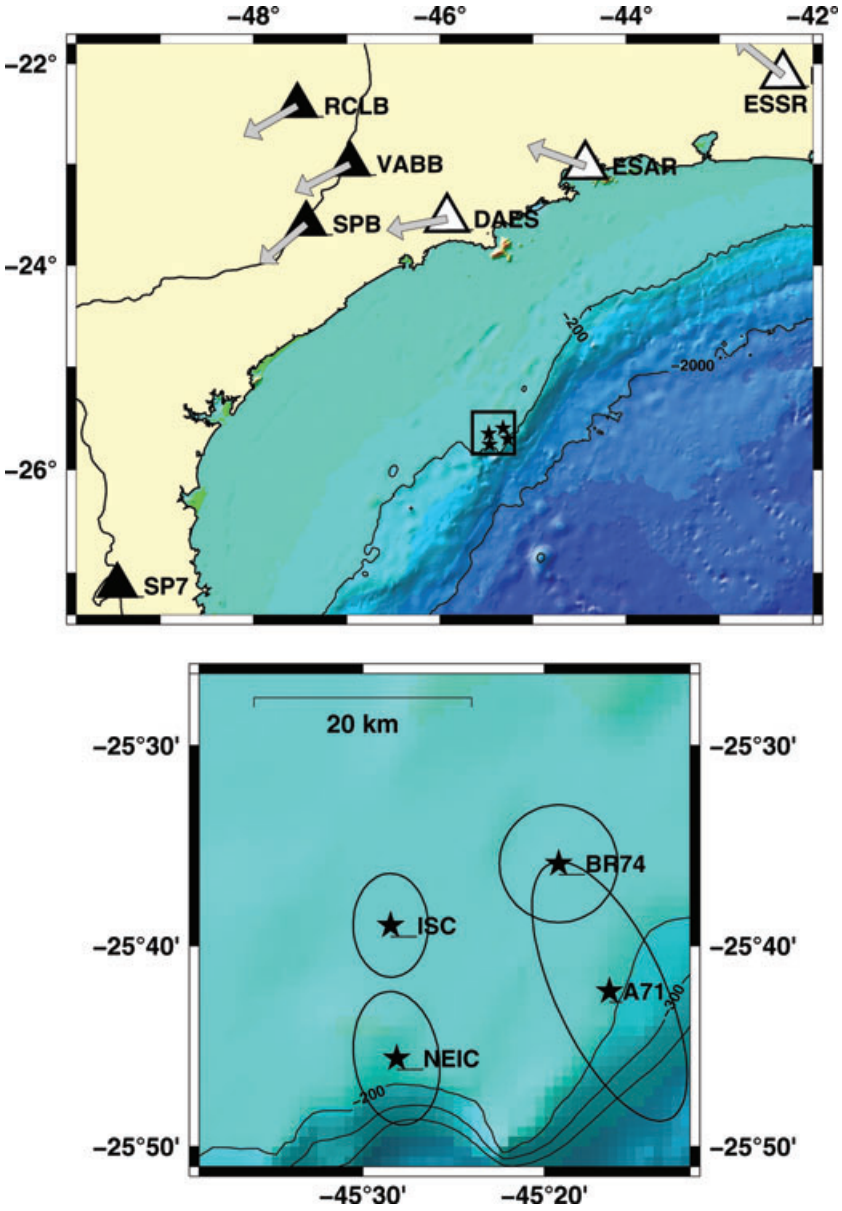



**Figure 4.** (a) Stations used for the regional epicentre determination. Solid triangles are stations with compressional (push) first *P*-wave motion; open triangles are dilatational (pull) first *P*-wave motion. Grey arrows indicate directions of the first SH motion shown in Fig. 4. Stars are epicentres of Table 1. (b) Detail of the various epicentral solutions shown in Table 1. Ellipses correspond to 90 per cent confidence limits for international agencies (NEIC and ISC), and standard error for the regional BR74 and A71 locations. Ellipse for A71 solution includes uncertainty of ±0.04 in the *Vp*/*Vs* ratio.

approximately 1 s, and $M_S$ with Rayleigh waves with periods close to 20 s. The USGS and ISC values were $m_b = 5.2$ and 5.0, and $M_S = 4.4$ and 4.2, respectively. The apparently large difference between $m_b$ and $M_S$ is common in intraplate areas and typical of other earthquakes in Brazil (e.g. Assumpção & Suárez 1988). It is usually interpreted as being due to relatively larger stress drops and smaller rupture areas, compared to interplate earthquakes, which cause relatively higher radiated energy in the short-period band where the $m_b$



Downloaded from http://gji.oxfordjournals.org/ at Universidade Estadual Paulista JÃºlio de Mesquita Filho on July 30, 2013

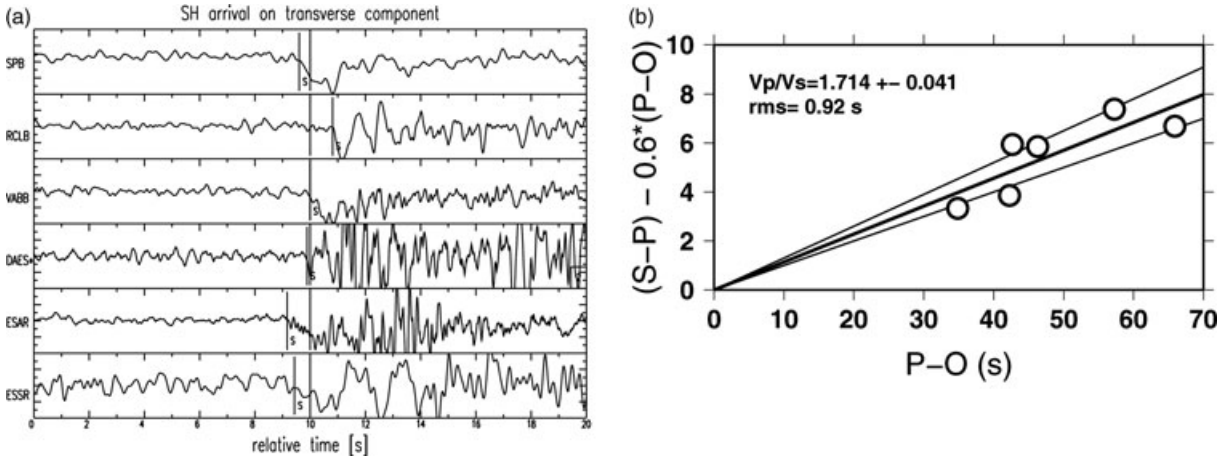



**Figure 5.** (a) Arrival of the SH wave (Sn-wave in the horizontal transverse component) at the best regional stations shown in Figure 2). Seismograms were converted to displacement and aligned according to the expected *S*-wave arrival time (10 s in the window). Note consistent negative first motion at all stations (i.e. first SH motion to the left). Amplitudes not to scale. (b) Wadati diagram with the SH arrivals from Fig. 5a. Size of circles are approximate reading errors of ±0.2 to 0.3 s. Thick solid line is the best-fitting *Vp*/*Vs* ratio of 1.714. Thin lines show *Vp*/*Vs* ratios of 1.70 and 1.73 for reference. Positive residuals are from stations to the North and NE (DAES, ESAR and ESSR), negative residuals are from NW stations (SPB, VABB, RCLB), indicating lateral variation in the regional structure.

is measured. However, as will be seen later, the stress drop for the São Vicente event is not particularly high. The regional magnitude ($m_R$) determined with 11 Brazilian stations was 5.05 ± 0.09 (*SD*). The Brazilian regional magnitude (Assumpção 1983) is equivalent to the teleseismic $m_b$ magnitude, on average. However, Barcelos *et al.* (2010) showed that $m_R$ tends to be lower than $m_b$ for dip-slip earthquakes (reverse or normal faulting with ∼45° dipping nodal planes) and $m_R > m_b$ for strike-slip earthquakes (near vertical null axis). For the São Vicente earthquake $m_R \approx m_b$, which is consistent with the uncommon focal mechanism shown below.

### 2.3 Focal depth

The São Vicente earthquake was also recorded by the best stations in North America and Africa. Fig. 6a shows records of the African stations where the wave first motion is clearly downwards (pull). Also, another clear phase can be seen at approximately 7.8 s after the direct *P*, which is the surface reflection *pP*. Stations in North America, on the other hand, had a consistent upwards *P* wave first motion (push), but very weak *pP* reflection (Fig. 6b). The time difference *pP*–*P* (from African, Antarctica and some North American stations), together with the *P*-wave velocity profile in the epicentral area (Fig. 7a), places the hypocentre at a depth of 17 km, that is in the lower crust well below the sedimentary pack. This depth is well constrained by these *pP* phases (Fig. 7b) and must be taken into account when correlating the earthquake with faults mapped in the sedimentary layers. The geological transect (Fig. 2) shows the hypocentre in the lower crust.

## 3 FOCAL MECHANISM

### 3.1 *P*-wave polarities

*P*-wave polarities of all regional (SE Brazil) and teleseismic stations (Fig. 8) show a clear nodal plane approximately oriented N–S. The other nodal plane (with approximately E–W orientation, dipping south was obtained by fitting the amplitude ratios of *pP*/*P* phases using the grid-search method of Assumpção & Suárez (1988). While the direction of the vertical, NNW–SSE trending plane is well constrained by the *P*-wave polarities, the orientation of the other subhorizontal plane is not well constrained and could vary by approximately 10°–20°. The left-lateral first motion of the *SH* wave at the regional stations (Fig. 5) is consistent with the nodal plane solution of Fig. 8.

Another confirmation of the focal mechanism solution can be seen with a more detailed analysis of the *pP* phase at the African stations. We stacked all records from the African stations (Fig. 8) after correcting the trace for the slight normal moveout between *pP* and *P* due to different epicentral distances (as seen in Fig. 7b). The stacked trace is in the middle of Fig. 9. To better identify the arrival of the *pP* wave, we removed the source signature by deconvolving the first *P* arrival from the whole trace. The *pP* phase exhibits a sharp positive peak, with the same polarity of the direct *P* wave. This is what would be expected for a dip-slip focal mechanism with a vertical nodal plane. The *pP* phase recorded at the African stations leaves the source as a compressional pulse upwards but changes polarity in the surface reflection and reaches the stations with the same polarity as the direct *P* wave.

### 3.2 Moment tensor inversion

The four closest broad-band stations, at distances between 310 and 420 km (SPB, ESAR, VABB and RCLB, shown in Fig. 3), were used to determine a moment tensor solution. We used the inversion program TDMT_INV (Dreger 2003; Minson & Dreger 2008) which calculates the complete Green's functions for a point source (no source time function is inverted for). The displacement seismograms were filtered in the range 20–50 s, much longer than the expected duration of the source time function of a magnitude 5 $m_b$ event (about 1 s). For each of the four stations a separate 1-D average velocity model was used based on the Rayleigh- and Love-wave group velocities. No isotropic component was allowed in the moment tensor inversion, only double-couple and CLVD components. The earthquake depth was fixed at 17 km.



Downloaded from http://gji.oxfordjournals.org/ at Universidade Estadual Paulista JÃºlio de Mesquita Filho on July 30, 2013

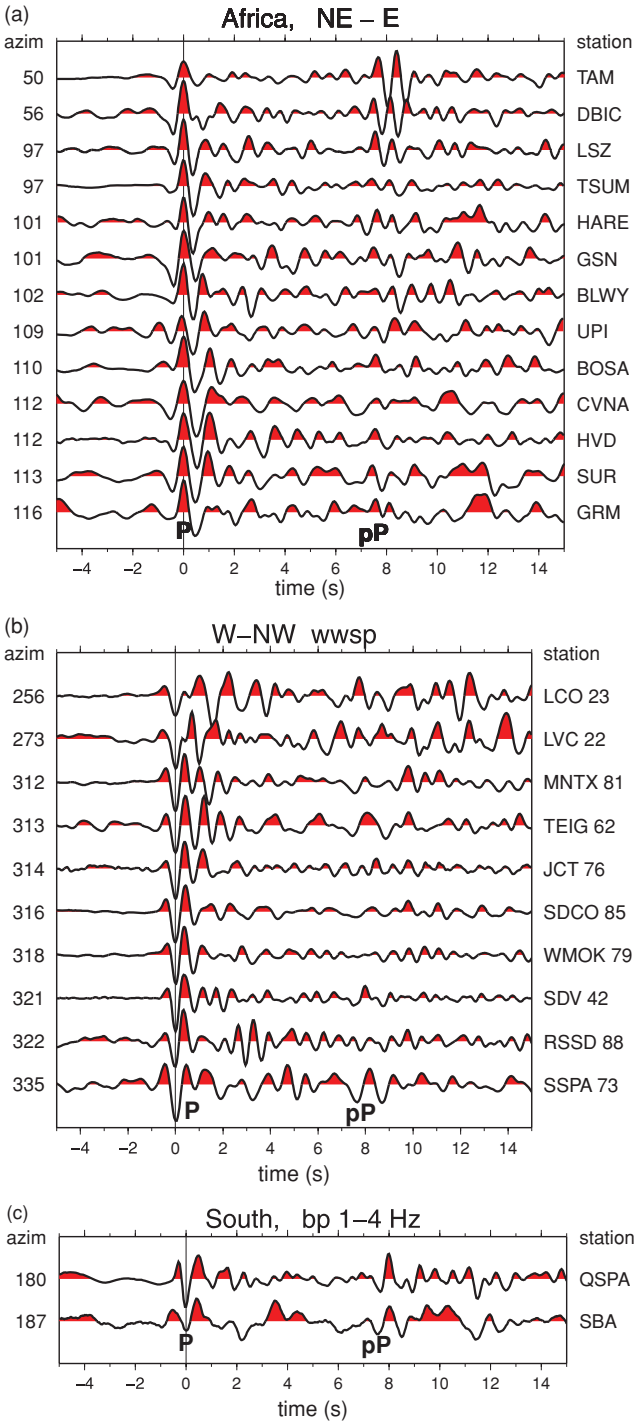



**Figure 6.** *P* and *pP* phases for stations at teleseismic distances. Numbers on the left are station azimuth measured at the epicentre; station names are on the right. Records are aligned by the second peak (or trough) with larger amplitude. (a) African stations to the NE and East of the epicentre showing *P*-wave first motion downwards (pull). (b) North American stations to the W-WNW of the epicentre, showing *P*-wave first motion upwards (push). (c) Antarctic stations to the south with upwards first motion. Approximately 8 s after the direct *P* wave, the surface reflexion *pP* can be seen, especially at the African and Antarctic stations. The *pP-P* difference gives a hypocentral depth of 17 km. Traces for (a) and (b) simulate a short-period WWSSN response. For (c) the traces were filtered with a causal band-pass of 1–4 Hz. Filters were chosen to best enhance the *pP* phase.

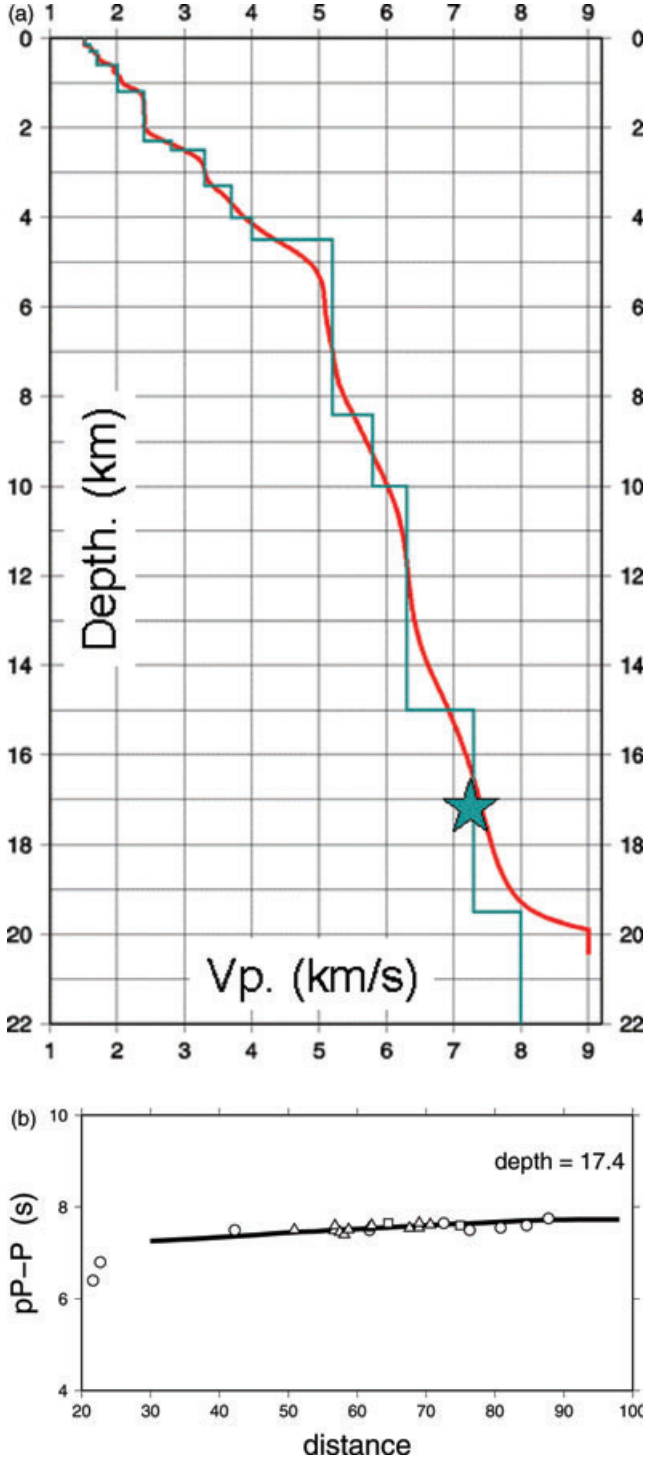



**Figure 7.** (a) *P*-wave velocity profile at the epicentral area (red line) and the equivalent plane-layer model (blue line) used to estimate the focal depth at 17.4 km (star). (b) Fit to the *pP-P* times read from seismograms shown in Figure 5. Circles are data from North American stations, triangles from African stations and squares from Antarctic stations. The solid line is the theoretical time using the IASP91 tables for the slowness and the crustal velocity model (a) for the *pP-P* time difference. Data near 20° are not reliable because of possible interference with triplication phases from the upper-mantle transition zone.

Downloaded from http://gji.oxfordjournals.org/ at Universidade Estadual Paulista JÃºlio de Mesquita Filho on July 30, 2013

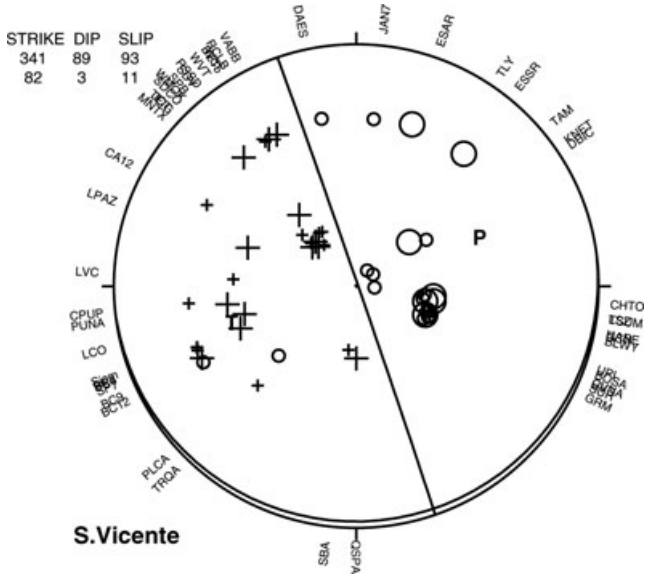



**Figure 8.** Focal mechanism solution of the 2008 São Vicente earthquake. Crosses and circles indicate upwards (push) and downwards (pull) *P*-wave first motions, respectively. Large and small symbols indicate more and less clear polarities. '*P*' and 'T' indicate the orientation of the stresses released by the event. The fault plane can be the vertical, NNW-striking plane, or the (almost horizontal) South dipping plane.

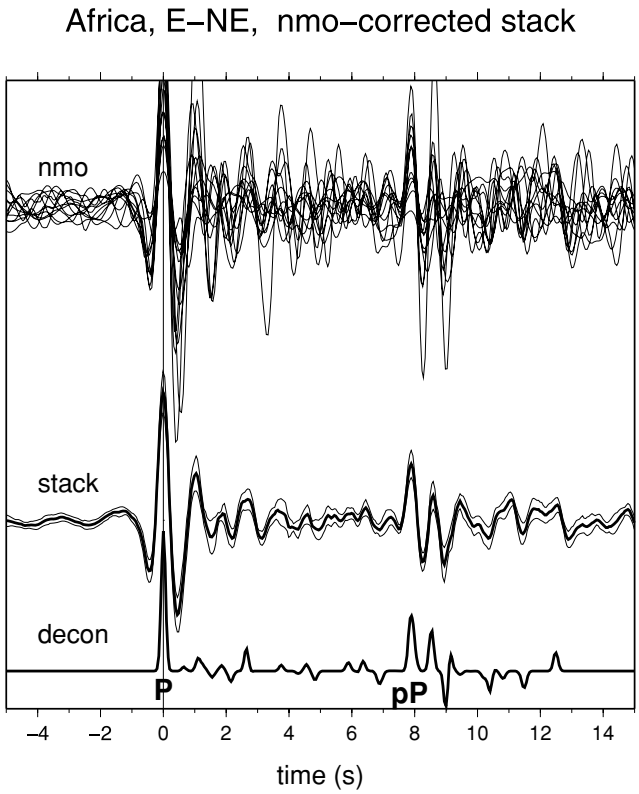



**Figure 9.** Enhancement of the depth phase *pP*. Top traces are the raw seismograms of each African station corrected for normal move-out to align the *pP* phase with normalized amplitudes. Middle traces are the stacked (average, thick line) and standard deviation (thin lines) of the traces above. Bottom trace is deconvolved from the first *P*-wave signal to remove the source signature and instrument effects; note the *pP* phase appears as a positive peak (i.e. same polarity as the first arrival), consistent with the focal mechanism solution.

Fig. 10 shows the inverted solution and the fit to the observed filtered traces. The fit of the synthetic to the observed traces corresponds to a variance reduction of 88 per cent. The best double couple (strike 346°, dip 81°, rake 76°) shows a near-vertical nodal plane quite consistent with the previous solution based only on the *P*-wave polarities, as shown in Fig. 8 (which had strike 341°, dip 89°, rake 93°). Sensitivity tests of the solution show that the small CLVD component (only 8 per cent) is not significant. The seismic moment was well defined at $0.14 \times 10^{17}$ N.m, giving a moment magnitude of $M_w = 4.7$.

The use of only *P* and *S* polarities, or waveform inversion, cannot resolve the ambiguity of the two nodal planes, and we cannot identify which is the fault plane. Two interpretations are therefore possible: (1) the fault plane is the vertical NNW–SSE oriented nodal plane, and the W side of the fault moves down, or (2) the fault is the subhorizontal plane (strike not well defined, but probably dipping slightly to the NW as shown in Fig. 10) with the upper block moving to the east.

Irrespective of the identification of the fault plane, a focal mechanism with vertical and horizontal nodal planes is very rare. The vast majority of crustal earthquakes have subhorizontal or vertical *P*- and *T*-axes. For the São Vicente earthquake, the directions of the *P*- and *T*-axes, the directions of the compressional and extensional stresses released by the earthquake, are clearly different from the other three focal mechanisms in the SE continental margin shown in Fig. 1(a). All other mechanisms were reverse faulting on planes dipping approximately 45° with horizontal compressional *P*-axes and vertical extensional *T*-axes. The uncommon focal mechanism of the 2008 earthquake probably indicates that the principal stresses acting at the hypocentral depth are not horizontal and vertical, as discussed later.

### 3.3 Stress drop

Stress drop ($\Delta\sigma$) was calculated by using an approximate estimate of source radius based on the duration of an assumed triangular source time function. The short-period teleseismic *P* waveform (stacked trace from the African stations, Fig. 9) was best modelled with a triangular source time function with 0.45 s of half-duration and an effective upper-mantle attenuation given by $t^* = 0.25$ (Fig. 11). The radius of a circular rupture area ($r$) can be estimated assuming a rupture speed about 0.8 the shear wave speed at the source (as used by Assumpção & Suárez 1988): $r = 0.8 \times 4.2$ km s$^{-1}$ $\times$ 0.45 s $= 1.5$ km. Assuming Brune's (1970) model for a circular source area, the stress drop is $\Delta\sigma = (7/16)\, Mo/r^3 = 1.8$ MPa (18 bar). This value is relatively low for an intraplate event. Global estimates of stress drops by Allmann & Shearer (2009), also using Brune's (1970) model, showed that $\Delta\sigma$ ranges from 0.1 to 100 MPa. Intraplate stress drops vary mostly between 1 and 40 MPa with a median value of 6 MPa, higher than the median value of 3.3 MPa for interplate earthquakes. The stress drop of 1.8 MPa for the São Vicente earthquake is in the lower end of the 'typical' range for intraplate events. The method we used is very approximate and strongly dependent on the estimated source radius. For source durations between 0.35 and 0.45 s (within the trade-off between duration and attenuation, as seen in the grid search of Fig. 11a), $\Delta\sigma$ would range from 1 to 4 MPa (10–40 bars). Stress drops for other Brazilian continental intraplate events range from 25 to 100 MPa as estimated by Assumpção & Suárez (1988) using exactly the same method. Despite the inherent large uncertainties of stress drop estimates, it seems the stress drop of the 2008

Downloaded from http://gji.oxfordjournals.org/ at Universidade Estadual Paulista JÃºlio de Mesquita Filho on July 30, 2013

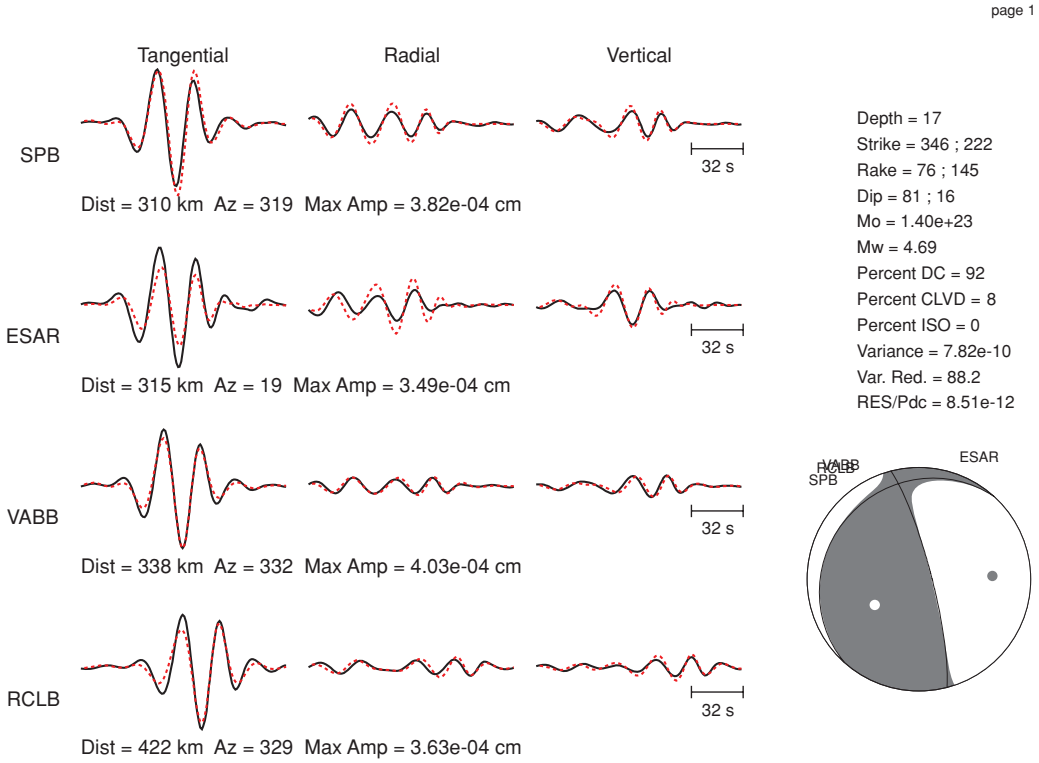



**Figure 10.** Moment tensor solution using the four closest broad-band regional stations. Solid black lines are the observed displacement records, dashed red lines are the synthetic seismograms. Each trace is 130 s long.

offshore São Vicente earthquake was smaller than other continental earthquakes in Brazil.

## 4 DISCUSSION

### 4.1 Stresses

Related to the stresses released by the earthquake, the *P*-axis orientation may differ from the direction of the tectonic principal maximum compressional stress (*S1*) acting in the crust. However, the extended crust beneath the continental shelf is expected to be highly fractured and faulted. In this case, earthquakes likely occur in weak fracture planes favourably oriented with respect to the tectonic stresses. For weak, pre-existing faults the most favourable orientation of the maximum principal compression is approximately 30° from the fault plane. If we assume that the fault is the NNW-striking vertical nodal plane (Fig. 8), the most favourable orientation for the maximum principal compression (*S1*) would be approximately ENE with a 70° plunge (30° from the fault).

The largest earthquakes in the continental shelf occur preferentially along the continental slope (Fig. 1) where sediment thickness tends to be largest. This is usually attributed to a significant contribution of flexural stresses from sediment load which amplify the regional stresses from plate-wide forces (e.g. Cleotingh *et al.* 1984, 1989; Stein *et al.* 1989; Watts *et al.* 2009). The load of the total sedimentary pack (up to ∼8 km for the Santos Basin) can produce flexural stresses several times higher than the yield stresses of crustal rocks. This indicates that during the ∼100 Ma evolution of the passive margin, the stresses from the accumulation of sediments are released almost continuously in faulting processes. The current flexural stresses are sustained only by the more recent sedimentation. Fig. 12 shows that the 2008 epicentre occurred at the northern edge of the sedimentary pack deposited since the Upper Oligocene.

Modelling of flexural stresses caused by sediment load (e.g. Cloetingh *et al.* 1984, 1989; Driscoll & Karner 1994; Watts *et al.* 2009) or intracrustal load (e.g. Zoback & Richardson 1996) show that right beneath the maximum load the crustal stresses are compressional (i.e. *S1* is horizontal). Away from the load, near the peripheral bulge, stresses in the upper crust change to extensional (i.e. *S3* is horizontal and *S1* is vertical). Below the neutral plane of the flexed plate, the stresses are opposite. However, in the transition between horizontal compression and horizontal extension, the crustal stresses rotate so that *S1* plunges away from the maximum load. This pattern is summarized in the conceptual diagram of Fig. 13, which was based on the calculated models of Cloetingh *et al.* (1989), Zoback & Richardson (1996) and Watts *et al.* (2009). We suggest that the 2008 earthquake occurred in such transition zone where *S1* is steeply dipping away from the maximum load, approximately towards the NE, due to the sediment load that was preferentially concentrated SW of the epicentre as shown in Fig. 12.

### 4.2 *pP* reverberation and epicentral uncertainty

A careful look at the *pP* wave in the stacked, deconvolved trace of Fig. 9 shows a large positive peak (7.9 s after the direct *P* and interpreted as the *pP* phase) followed by one positive peak and another negative peak. An alternative interpretation for these three peaks is that the first large peak is the reflection from the sediment/water interface (called '*bP*' by Assumpção 1998a); the second positive peak is the reflection from the water surface (the true *pP*) and the negative peak the water reverberation (*wwP*). The polarities of the three peaks are consistent with this interpretation. However, the time difference between each peak (about 0.55 s) implies a



Downloaded from http://gji.oxfordjournals.org/ at Universidade Estadual Paulista JÃºlio de Mesquita Filho on July 30, 2013

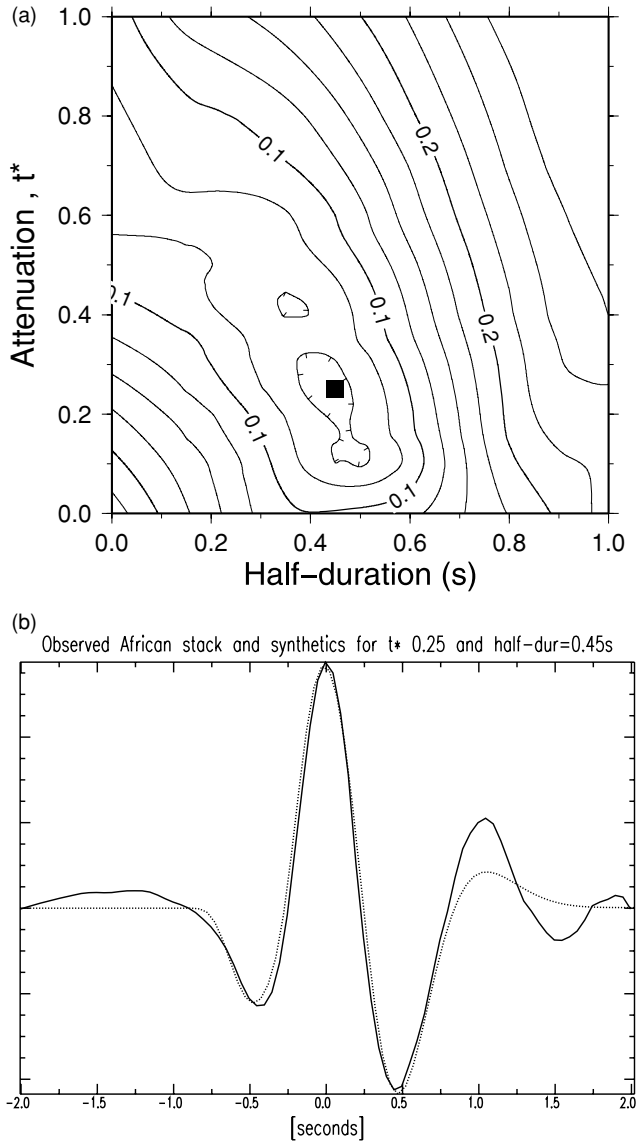



**Figure 11.** Modelling of the teleseismic short-period *P* waveform. (a) Grid search for the best-fitting parameters: half-duration of a triangular source time function and upper-mantle effective attenuation $t^*$; contours show rms misfit; solid square shows the minimum misfit. Note the trade-off between attenuation and source duration. (b) Comparison between the observed African stacked trace with WWSSN response (solid line) and the synthetic trace with 0.45 s half-duration and $t^* = 0.25$ (dashed line).

water depth of approximately 400 m. This requires the ISC epicentre (Fig. 4b) to be more than 20 km off from the true location, but remains consistent with the National Earthquake Information Center (NEIC) epicentre or the regional A71 solution. One problem of this interpretation is that the *bP* phase usually has lower amplitude than the true *pP* reflected from the water surface because of a lower impedance contrast. This issue will require more work in the future.

### 4.3 Earthquake versus slump

Some large events occurring near the continental slope have been interpreted as huge slumps instead of tectonic earthquakes, such as the magnitude 7.2 Grand Banks event of 1929 off the eastern coast of Canada. The Grand Banks seismic event was interpreted as the slump itself (Hasegawa & Kanamori 1987; Hasegawa & Herrmann 1989) or as a deep crustal, complex earthquake, which caused the sediment slumping (Bent 1995). Berrocal *et al.* (1996) suggested that the 1990 Rio Grande do Sul (Fig. 1a) event could have been a marine landslide. The 2008 São Vicente earthquake occurred near a major canyon in the continental slope, with geological evidence of past slumps. For this reason some authors have suggested that the São Vicente event could have been a slump and not an earthquake. Clearly, these hypotheses have important implications for seismic risk estimates along the continental shelf. However, the focal mechanisms and hypocentral depths of the 1988 event in Uruguay, the 1990 event in Rio Grande do Sul (Assumpção 1998a) and the 2008 São Vicente event clearly show that, thus far, no large earthquake in the SE Brazilian continental shelf can be attributed to a slump. Instead, these events were earthquakes caused by failure of deep faults under the present tectonic stresses affecting weak zones of the crust. In addition, both the *P*-wave polarity data (Fig. 8) and the moment tensor solution (Fig. 10) show that a pure double couple mechanism can completely explain all the observations. Any seismic contribution from a slump component would be very small and probably not resolvable with the present data.

### 4.4 The 2008 earthquake and geological faults

Correlation of earthquakes with geological/geophysical structural features is known to be a difficult task, especially in intraplate areas where the number of earthquakes is few and statistical variability makes it difficult to reach robust conclusions. For this reason we refrain from trying to associate the 2008 earthquake with any specific fault or structures, especially in view of the epicentre uncertainty. However, it is interesting to note that the 2008 São Vicente earthquake occurred near major structures of the Santos basin, such as the NW–SE Capricornio Lineament (Bueno 2004; Bueno *et al.* 2004) shown in Fig. 1(b), as well as the Merluza graben (Fig. 2) a N–S feature in southern to central Santos Basin marked by extensional faults affecting the base of the salt. Although the NNW–SSE orientation of the vertical nodal plane could favour structures such as the Merluza graben, many listric faults mapped in the upper crust tend to a horizontal orientation in the lower crust, so that the horizontal nodal plane cannot be ruled out as a possible fault plane purely on geometrical grounds.

## 5 CONCLUSIONS

The 2008 São Vicente earthquake had a hypocentre in the lower crust (17 km focal depth) approximately 12 km below the sedimentary layers. The focal mechanism indicates two possibilities for the orientation of the fault plane: a vertical NNW–SSE striking plane with vertical dip-slip motion, or a subhorizontal plane with lateral motion. Both the focal mechanism and the hypocentral depth rule out the interpretation of a slump in the continental slope as the major cause of the observed seismic waves.

Flexural stresses due to sediment load along the continental shelf probably play a major role in causing the São Vicente earthquake as well as most of the seismicity along the SE continental shelf. We suggest that a rotation of the flexural stresses in the transition zone between the compressional field right beneath the maximum load and the extensional stresses near the peripheral bulge causes the unusual orientation of the nodal planes.

Downloaded from http://gji.oxfordjournals.org/ at Universidade Estadual Paulista JÃºlio de Mesquita Filho on July 30, 2013

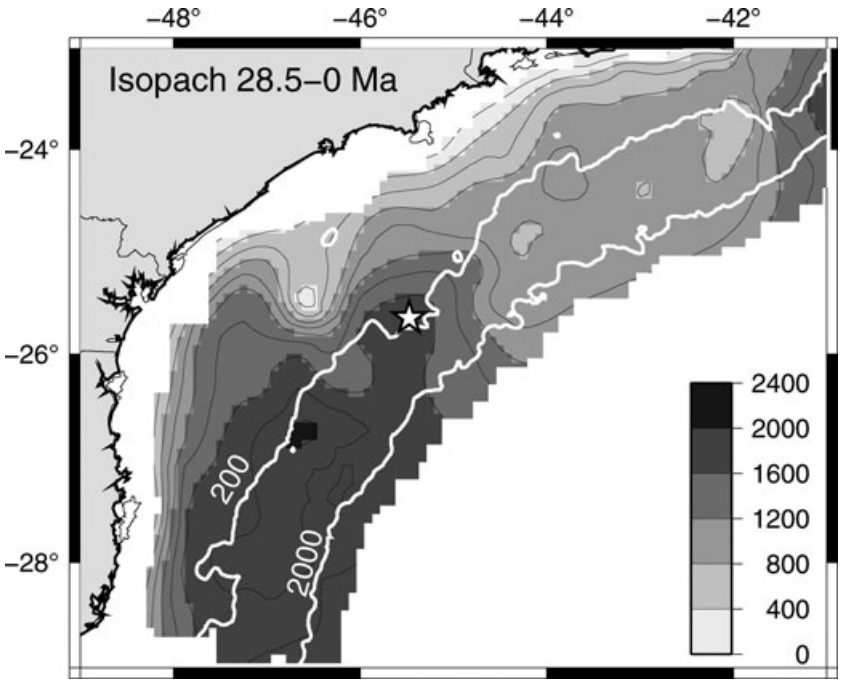



**Figure 12.** Sediment thickness (grey scale in the ocean, in metres) since the Upper Oligocene (28.5 Ma to present, data from Chang 2003). Star is the ISC epicentre showing that the event occurred at the edge of a long sedimentary load. White lines are the 200 and 2000 m water depth.

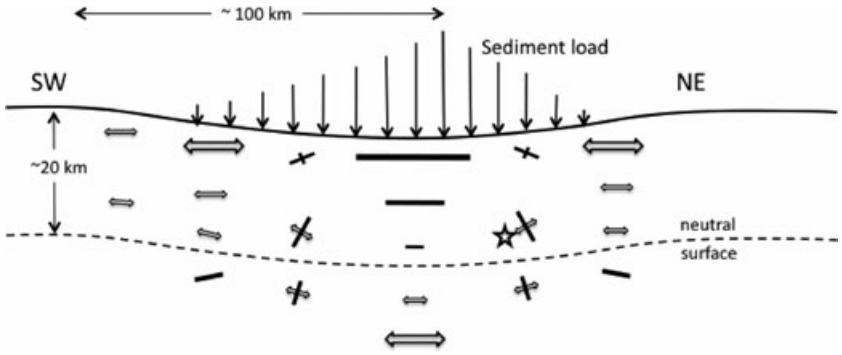



**Figure 13.** Conceptual model of flexural stresses with steeply dipping S1 compressional axis in the transition zone between horizontal compression beneath the maximum load and horizontal extension near the peripheral bulge. Vertical thin arrows represent the sediment load on a flexing plate. Solid bars denote compressional principal stresses, open double arrows denote extensional principal stresses. Stress pattern is typical of numerical models such as those of Cloetingh *et al.* (1989), Zoback & Richardson (1996) and Watts *et al*. (2009). Star denotes event location.

## ACKNOWLEDGMENTS

This paper was only possible due to the high quality data gathered from several seismographic stations both in Brazil and abroad. We thank Jesús Berrocal and Afonso Lopes for data from ESAR and ESSR stations; Andy Nyblade (Penn State) for data from the Africa-Array project; Patricia Alvarado (San Juan) and Eric Sandvol (Missouri) for data from the Sierra and Puna projects, respectively; Lucas Barros and George França for data from the University of Brasília stations. Data from the IRIS/DMC was extensively used. The moment tensor was computed using the mtpackagev3.0 developed by Douglas Dreger and Sean Ford of the Berkeley Seismological Laboratory, and Green's functions computed with the FKRPROG software developed by Chandan Saikia. IRIS/PASI program provided valuable training. We thank Petrobrás for information on the crustal velocity profile near the epicentre. This work was carried out with CNPq grants 309724/2009–0 and 30.0460/2010–4.

## REFERENCES

Allmann, B.P. & Shearer, P.M., 2009. Global variations of stress drop for moderate to large earthquakes, *J. geophys. Res.,* **114,** B01310, doi:10.1029/2008JB005821.

Assumpção, M., 1983. A regional magnitude scale for Brazil, *Bull. seism. Soc. Am.,* **73,** 237–246.

Assumpção, M., 1998a. Seismicity and stresses in the Brazilian passive margin, *Bull. seism. Soc. Am.,* **88**(1), 160–169

Assumpção, M., 1998b. Focal mechanisms of small earthquakes in SE Brazilian shield: a test of stress models of the South American plate, *Geophys. J. Int.,* **133,** 490–498.

Assumpção, M. & Suárez, G., 1988. Source mechanisms of moderate-size earthquakes and stress orientation in mid-plate South America, *Geophys. J.,* **92,** 253–267.

Barcelos, A., Assumpção, M. & Pirchiner, M., 2010. Magnitude determination of regional earthquakes in Brazil: a comparison of the new IASPEI magnitude formulas, *EOS, Trans. AGU,* **91**(26), Meeting Supplement, Abstract, Iguassu Falls, Brazil, 2010 August 8–13.



Downloaded from http://gji.oxfordjournals.org/ at Universidade Estadual Paulista JÃºlio de Mesquita Filho on July 30, 2013

Bent, A.L., 1995. A complex double-couple source mechanism for the Ms 7.2 1929 Grand Banks earthquake, *Bull. seism. Soc. Am.,* **85,** 1003–1020.

Berrocal, J., Fernandes, C., Bassini, A. & Barbosa, J.R., 1996. Earthquake hazard assessment in southeastern Brazil, *Geofis. Int.,* **35,** 257–272.

Bondár, I., Myers, S.C., Engdahl, E.R. & Bergman, E.A., 2003. Epicentre accuracy based on seismic network criteria, *Geophys. J. Int.,* **156,** 483–496.

Brune, J., 1970. Tectonic stress and spectra of seismic shear waves from earthquakes, *J. geophys. Res.,* **75,** 4997–5009. [Correction, 1971 *J. geophys. Res.*, **76**, 5002].

Bueno, G.V., 2004. Diacronismo de eventos no rifte Sul-Atlântico, *Bol. Geoc. Petrobras,* Rio de Janeiro, **12**(2), 203–229.

Bueno, G.V., Machado, D.L., Jr, Oliveira, J.A.B. & Marques, E.J.J., 2004. A influência do Lineamento de Capricornio na evolução tectono-sedimentar da bacia de Santos. *Abstracts*, *42nd Brazilian Geological Congress,* Araxá, MG, Brazil.

Bungum, H., Olesen, O., Pascal, C., Gibbons, S., Lindholm, C. & Vestøl, O., 2010. To what extent is the present seismicity of Norway driven by postglacial rebound? *J. Geol. Soc. Lond.,* **167,** 373–384.

Carminatti, M., Wolff, B. & Gamboa, L.A.P., 2008. New exploratory frontiers in Brazil, in *Proceedings of the 19th World Petroleum Congress,* Madrid, Spain, Abstracts CD, 11 pp.

Chang, H.K., 2003. *Mapeamento e Interpretação dos Sistemas Petrolíferos da Bacia de Santos*, http://www.anp.gov.br/brnd/round5/round5/Apres_SemTec/R5_Santos.pdf (accessed in 2011 February 16).

Chang, H.K., Kowsman, R., Figueiredo, A.M.F. & Bender, A.A., 1992. Tectonics and stratigraphy of the east Brazil rift system: an overview, *Tectonophysics,* **213,** 97–138.

Cloetingh, S.A.P.L., Wortel, M.J.R. & Vlaar, N.J., 1984. Passive margin evolution, initiation of subduction and the Wilson cycle, *Tectonophysics,* **109,** 147–163.

Cloetingh, S.A.P.L., Wortel, M.J.R. & Vlaar, N.J., 1989. On the initiation of subduction zones. *Pageoph,* **129,** 7–25.

Cobbold, P.R., Szatmari, P., Demercian, L.S., Coelho, D. & Rossello, E.A., 1995. Seismic experimental evidence for thin-skinned horizontal shortening by convergent radial gliding on evaporites, deep-water Santos Basin, *AAPG Memoir,* **65,** 305–321.

Dourado, J.C. & Assumpção, M., 2010. The 5.2 mb São Vicente earthquake of 2008 in the continental shelf off SE Brazil: using reflection seismic sections to constrain the fault plane, *AGU Meeting of the Americas, Iguassu Falls,* Brazil, 2010 August 8–13, Abstract.

Dourado, J.C., & Assumpção, M., 2011. The 5.2 mb São Vicente earthquake of 2008 in the continental shelf off SE Brazil: using reflection seismic sections to constrain the fault plane, *Rev. Bras. Geofísica,* submitted (in Portuguese).

Dreger, D.S., 2003. TDMT_INV: time domain seismic moment tensor inversion, in *International Handbook of Earthquake and Engineering Seismology,* Vol. 81B, p. 1627, Academic Press, London.

Driscoll, N.W. & Karner, G.D., 1994. Flexural deformation due to Amazon Fan loading: a feedback mechanism affecting sediment delivery to margins, *Geology,* **22,** 1015–1018, doi:10.1130/0091-7613(1994)022<1015:FDDTAF>2.3.CO;2

Feng, M., Van der Lee, S. & Assumpção, M., 2007. Upper mantle structure of South America from joint inversion of waveforms and fundamental-mode group velocities of Rayleigh waves, *J. geophys. Res.,* **112,** B04312, doi:10.1029/2006JB004449.

Gomes, B.S., 1992. Preliminary integration of marine gravimetric data of Petrobras and Leplac project: Campos, Santos and Pelotas basins, in *Proceedings of the 37th Brazilian Geological Congress,* 1, 559–560, São Paulo, SP, Brazil (in Portuguese).

Gomes, P.O., Kilsdonk, B., Minken, J., Grow, T. & Barragan, R., 2008. The outer high of the Santos Basin, Southern São Paulo Plateau, Brazil: pre-salt exploration outbreak, palaeogeographic setting, and evolution of the syn-rift structures, AAPG International Conference and Exhibition, Cape Town, South Africa, 2008 October 26–29, Abstracts CD, http://www.searchanddiscovery.net/documents/2009/10193gomes/images/gomes.pdf (last accessed 2011 September 17).

Hasegawa, H.S. & Herrmann, R.B., 1989. A comparison of the source mechanism of the 1975 Laurentian Channel earthquake and the tsunamigenic 1929 Grand Banks event, in *Earthquakes at North-Atlantic Passive Margins: Neotectonics and Postglacial Rebound,* pp. 547–562, eds Gregersen, S. & Basham, P.W., Kluwer Academic, Boston, MA.

Hasegawa, H.S & Kanamori, H., 1987. Source mechanism of the magnitude 7.2 Grand Banks earthquake of November 1929: double couple or submarine landslide? *Bull. seism. Soc. Am.,* **77,** 1984–2004.

ISC, 2011. *International Seismological Centre*, *On-line Bulletin,* http://www.isc.ac.uk (last accessed 2011 September 17).

Johnston, A.C., 1989. The seismicity of stable continental interiors, in *Earthquakes at North-Atlantic Passive Margins: Neotectonics and Postglacial Rebound,* pp. 299–327, eds Gregersen, S. & Basham, P.W., Kluwer Academic, Boston, MA.

Johnston, A.C. & Kanter, L.R., 1990. Earthquakes in stable continental crust, *Sci. Am.,* **262,** 68–75.

Kwitko, R. & Assumpção, M., 1990. Modelo de velocidades para o manto superior no Brasil e determinação de epicentros regionais, in *Proceedingsof the 36th Congr. Bras. Geol.,* Natal, RN, 5, pp. 2464–2469.

Mendiguren, J.A. & Richter, F.M., 1978. On the origin of compressional intraplate stresses in South America, *Phys. Earth planet. Inter.,* **16,** 318–326.

Minson, S.E. & Dreger, D.S., 2008. Stable inversions for complete moment tensors, *Geophys. J. Int.,* **174,** 585–592, doi:10.1111/j.1365-246X.2008.03797.x.

Mohriak, W.U., 2001. Salt tectonics, volcanic centers, fracture zones and their relationship with the origin and evolution of the South Atlantic Ocean: geophysical evidence in the Brazilian and West African margins, in *Proceedings of the 7th Internaional Congress of the Brazilian Geophysical Society*, Salvador, Bahia, Brazil, 2001 October 28–31, Expanded Abstract, pp. 1594–1597.

Mohriak, W.U., 2004. Recursos energéticos associados à ativação tectônica mesozóico-cenozóica da América do Sul, in *Geologia do Continente Sul-Americano: Evolução da Obra de Fernando Flávio Marques de Almeida,* Vol. XVIII, pp. 293–318, eds Mantesso–Neto, V. Bartorelli, A., Carneiro, C.D.R. & Brito-Neves, B.B., Beca Produções Culturais Ltd., São Paulo.

Mohriak, W.U. *et al*., 1995. Salt tectonics and structural styles in the deep-water province of the Cabo Frio region, Rio de Janeiro, Brazil, *AAPG Memoir,* **65,** 273–304.

Mohriak, W.U., Nemcok, M. & Enciso, G. 2008. South Atlantic divergent margin evolution: rift-border uplift and salt tectonics in the basins of SE Brazil, *Geol. Soc. Lond. Spec. Pub.,* **294,** 365–398.

Mohriak, W.U., Nóbrega, M. Odegard, M.E., Gomes, B.S. & Dickson, W.G., 2010. Geological and geophysical interpretation of the Rio Grande Rise, south-eastern Brazilian margin: extensional tectonics and rifting of continental and oceanic crusts, *Pet. Geosci.,* **16,** 231–245. doi:10.1144/1354-079309-910.

Rocha, M.P. Schimmel, M. & Assumpção, M., 2011, Upper-mantle seismic structure beneath SE and Central Brazil from P- and S-wave regional traveltime tomography, *Geophys. J. Int.,* **184,** 268–286, doi:10.1111/j.1365-246X.2010.04831.x.

Riccomini, C. & Assumpção, M., 1999. Quaternary tectonics in Brazil. *Episodes,* **22**(3), 221–225.

Schulte, S.M. & Mooney, W.D., 2005. An updated global earthquake catalogue for stable continental regions: reassessing the correlation with ancient rifts. *Geophys. J. Int.,* **161,** 707–721.

Stein, S., Cloetingh, S., Sleep, N.H. & Wortel, R., 1989. Passive margin earthquakes, stresses and rheology, in *Earthquakes at North-Atlantic Passive Margins: Neotectonics and Postglacial Rebound,* pp. 231–259, eds Gregersen, S. and Basham, P.W., Kluwer Academic, Boston, MA.

Sykes, L., 1978. Intraplate seismicity, reactivation of pre-existing zones of weakness, alkaline magmatism, and other tectonism postdating continental fragmentation, *Rev. geophys. Space Phys.,* **16,** 621–688.

Watts, A.B., Rodger, M., Peirce, C., Greenroyd, C.J. & Hobbs, R.W., 2009. Seismic structure, gravity anomalies, and flexure of the Amazon continental margin, NE Brazil, *J. geophys. Res.,* **114,** B07103, doi:10.1029/2008JB006259.

Downloaded from http://gji.oxfordjournals.org/ at Universidade Estadual Paulista JÃºlio de Mesquita Filho on July 30, 2013

Zalán, P.V., Severino, M.C.G., Oliveira, J.A.B., Magnavita, L.P., Mohriak, W.U., Gontijo, R.G., Viana, A.R. & Szatmari, P., 2009. Stretching and thinning of the upper lithosphere and continental-oceanic crustal transition, *AAPG International Conference & Exhibition*, 2009 November 15–18, Abstracts Volume, 653274.

Zoback, M.L, 1992. Stress field constraints on intraplate seismicity in Eastern North America, *J. geophys. Res.,* **97,** 11761–11782.

Zoback, M.L. & Richardson, R.M., 1996. Stress perturbation associated with the Amazonas and other ancient continental rifts, *J. geophys. Res.,* **101,** 5459–5475.

Downloaded from http://gji.oxfordjournals.org/ at Universidade Estadual Paulista JÃºlio de Mesquita Filho on July 30, 2013